Applied Catalysis B: Environmental 119–120 (2012) 267–272

Contents lists available at SciVerse ScienceDirect

Applied Catalysis B: Environmental

journal homepage: www.elsevier.com/locate/apcatb

Hierarchical P/YPO_4 microsphere for photocatalytic hydrogen production from water under visible light irradiation

Feng Wang, Chuanhao Li, Yecheng Li, Jimmy C. Yu*

Department of Chemistry and Institute of Environment, Energy and Sustainability, The Chinese University of Hong Kong, Shatin, New Territories, Hong Kong, China

ARTICLE INFO

Article history:
Received 9 December 2011
Received in revised form 3 March 2012
Accepted 9 March 2012
Available online 19 March 2012

Keywords:
Hydrogen production
Photocatalyst
Red phosphorus
Visible-light-driven
Yttrium phosphate

ABSTRACT

Hierarchical P/YPO_4 hollow microspheres are prepared by the reaction between amorphous red P and YCl_3 aqueous solution via a hydrothermal method. The final product consists of crystalline YPO_4 nanosheets and amorphous red phosphorus. Photocatalytic hydrogen formation measurements indicate that the P/YPO_4 composites exhibit higher activity than the individual components. The composite with 53 wt% YPO_4 is up to 6 times more active than red phosphorus under visible light irradiation. The formation mechanism of hierarchical microspheres and the enhanced photocatalytic activity are discussed.

1. Introduction

The depletion of fossil fuel reserves is one of the most urgent issues facing modern society. Solar-induced photocatalytic hydrogen production from water has been considered as a promising way to alleviate this problem [1–3]. For effective utilization of solar light, numerous attempts have been devoted to the exploration of novel visible-light-driven photocatalysts. These include non-metal or metal ion(s) doped metal oxides, oxynitride, oxysulfide photocatalysts, polymeric photocatalysts, and sensitized systems [4–6]. Red phosphorus has been discovered recently as a visible-light-driven photocatalyst for H_2 formation from water [7]. An attractive property of red phosphorus is a wide visible light absorption band. The absorption band edge is all the way to ~700 nm. However, the photocatalytic efficiency for H_2 formation over red P is relatively low, mainly due to a rapid recombination of photogenerated electrons and holes.

By coupling two different semiconductors together to form a composite, interesting and desirable properties can be obtained [8–10]. For photocatalytic applications, the interface(s) between different components could lead to effective separation of photogenerated carriers [11–14]. Generally, the composites are fabricated by the sequential growth of a second semiconductor on the active seeding photocatalysts [15,16]. For red phosphorus, it reacts with metal compounds to form phosphates or phosphides under suitable conditions [17,18]. This allows the development of a serial of interesting red P based functional composites.

In this work, hierarchical P/YPO_4 hollow microspheres are fabricated by the reaction between red P and YCl_3 aqueous solution via a hydrothermal method. The hierarchical microsphere product is assembled by crystalline YPO_4 nanosheets and amorphous red P. The formation mechanism is investigated by time-dependent experiments. Photocatalytic H_2 formation measurements show that the composites exhibit higher activity than the individual components.

2. Experimental

2.1. Sample preparation

Commercial red phosphorus was purified to remove surface oxidation before use. Typically, red P was dispersed in D.I. water. The suspension was put into a Teflon-lined stainless autoclave and maintained at 200 °C for 12 h. $YCl_3{\cdot}6H_2O$ (≥99.999%, w/w, Sigma–Aldrich) was used without further purification. P/YPO_4 hierarchical microspheres were fabricated by a hydrothermal method. In a typical synthesis, 0.3 g of $YCl_3{\cdot}6H_2O$ was dissolved in 15 mL of D.I. water, and then 0.3 g of purified red phosphorus was added. After ultrasonic for 5 min, the prepared solution was transferred into a preheated 200 °C oven for 20 h. After the reaction, resulted products in suspension were washed with D.I. water and ethanol. Finally, the products were dried under vacuum at 60 °C. Pure YPO_4

* Corresponding author. Tel.: +852 3943 6268; fax: +852 2603 5057.
E-mail address: jimyu@cuhk.edu.hk (J.C. Yu).

0926-3373/$ – see front matter © 2012 Elsevier B.V. All rights reserved.
doi:10.1016/j.apcatb.2012.03.011

was prepared via the same procedure as P/YPO_4 composites with an excess amount of $YCl_3{\cdot}6H_2O$.

2.2. Characterizations

The XRD patterns of the products were recorded by powder X-ray diffraction (XRD) with a Bruker D8 Advance diffractometer using Cu $K_{\alpha 1}$ irradiation (λ = 1.5406 Å). The general morphologies of the products were characterized by scanning electron microscopy (SEM, Quanta 400) and transmission electron microscopy (TEM) images (TEM, Tecnai F20 microscope) coupled with an energy-dispersive X-ray (EDX) spectrometer (Oxford Instrument). UV–vis diffuse reflectance spectra were collected by a UV–vis spectrophotometer (Cary 100 scan spectrophotometers, Varian). The Brunauer–Emmett–Teller surface areas were determined by nitrogen adsorption and desorption with a Micromertics ASAP 2010 analyzer. X-ray photoelectron spectroscopy (XPS) spectra were recorded by a PHI 5600 multi-technique system with a monochromatic Al K_α X-ray source (Physical Electronics). All the binding energies were referenced to the C1s peak at 284.8 eV of the surface adventitious carbon. The percentages of red P in P/YPO_4 composites were determined by a thermogravimeteric analyzer (TGA6, Perkin-Elmer) under N_2 flow (20 mL/min) with a heating rate of 10 °C/min.

2.3. Hydrogen production tests

The photocatalytic H_2 formation experiments were carried out in a Pyrex reaction cell connected to a closed gas circulation with an evacuation system. 50 mg of the sample were dispersed in 100 mL of aqueous solution containing 5 vol% methanol as a hole sacrificial agent. The suspension was purged with argon to remove dissolved air before irradiation. 1% Pt was loaded onto all samples by photoreduction of H_2PtCl_6 [19,20]. The amount of Pt was measured by an XPS analyzer (Fig. S1). The suspension was irradiated by a 300 W xenon lamp with a 400 nm cut-off filter and a water filter. The amounts of hydrogen generated from photocatalytic water reduction were measured by a Techcomp GC7900 gas chromatography with a TCD detector and a capillary column (Molecular Sieve 5 Å). High purity nitrogen gas was used as a carrier gas.

3. Experimental results and discussion

The powder X-ray diffraction (XRD) pattern provides crystallinity and phase information for the P/YPO_4 composite. All the diffraction peaks are readily indexed to the tetragonal YPO_4 (JCPDS No. 11-0254), as shown in Fig. 1a. The existence of red P in the composite can be confirmed by UV–vis diffuse reflectance spectra, colors of products and XPS spectra. As shown in Fig. 1b, pure YPO_4 is a white powder with no absorption in the visible range. The composite is a red powder with an absorption edge at about 700 nm. The chemical composition of the samples and the oxidation states of phosphorus are obtained from XPS analysis. The survey XPS spectrum reveals that the microspheres are composed of Y, P and O, as shown in Fig. 1c. In the high-resolution P 2p XPS spectrum, two peaks at the binding energies of ~134.7 eV and ~129.8 eV are observed (Fig. 1d), corresponding to the characteristic of P^{5+} in YPO_4 and elemental P, respectively [21,22]. No red P peak is observed in the XRD pattern, suggesting the amorphous structure of red phosphorus in the composite. These results indicate the prepared composite is composed of crystalline YPO_4 and amorphous red P.

The morphology and microstructure of the P/YPO_4 composite were recorded by using scanning electron microscopy (SEM) and transmission electron microscopy (TEM). Fig. 2a indicates that the product is composed of a large quantity of microspheres. The mean diameter of the microspheres is ~750 nm. The high-magnification SEM image shows all microspheres have a hierarchical architecture (Fig. 2b). TEM images in Fig. 2c and d clearly show the hollow nature of microspheres and suggest that the hierarchical structure is built from nanosheets. The average thickness of the sheets is about 15 nm. High-resolution TEM (HRTEM) image indicates the single crystallinity of the nanosheets, as shown in the inset of Fig. 2d. The periodic fringe spacing of ~3.5 Å corresponds to the interplanar spacing between the (0 1 2) planes of the tetragonal YPO_4. This agrees with the XRD results. However, it is difficult to show the distribution of red phosphorus in the microsphere by the conventional mapping method. This is due to the overlapping of the binding energy of P with that of Y (Fig. S2). Time-dependent experiments were carried out to understand the distribution of red P and the formation mechanism of the hierarchical microspheres.

Fig. 3 shows the SEM and TEM images of products obtained with different reaction times. They reveal a clear trend of morphology evolution. Microspheres are formed after reacting for 30 min, as shown in Fig. 3a and b. The microspheres are mainly composed of P as indicated by EDX analysis (data not shown). When the reaction proceeds to 1 h, needle-like YPO_4 is observed on the surface of the microspheres (Fig. 3c and d). As the reaction goes on, more YPO_4 are formed and the hollow structure could be seen (Fig. 3e and f). At last, hierarchical P/YPO_4 microspheres with sheet-like YPO_4 are formed (Fig. 3e and f). It is noted that the size of microspheres is different at different reaction stages. The size of microspheres is ~1050 nm at 0.5 h and increases to ~1450 nm at 1 h, beyond which it decreases. At the end of the reaction, the size of microspheres is ~750 nm. Besides, the evolution processes of the hierarchical P/YPO_4 composites also show that the amorphous red phosphorus mainly distribute in the inner layer of microspheres and connects with the crystalline YPO_4 nanosheets to form hierarchical microspheres.

Concerning the morphology evolution of the P/YPO_4 microspheres, the reaction between YCl_3 and P should have played a key role, because no other templates and surfactants are used in our reaction system. The formation of P/YPO_4 composite can be understood by the following equations:

$$8P + 12H_2O \xrightarrow[50\,^\circ C]{O_2} 5PH_3 + 3H_3PO_4 \quad (a)$$

$$YCl_3 + H_3PO_4 \rightarrow YPO_4\downarrow + 3HCl \quad (b)$$

It is known that red P has a disproportionation with the formation of phosphine and phosphate acid in the presence of O_2 and moisture at elevated temperatures (Eq. (a)) [23,24]. In the presence of YCl_3, the H_3PO_4 formed in the first reaction could be consumed immediately with the formation of YPO_4 precipitated (Eq. (b)). Accordingly, the dissociation of red phosphorus is promoted. At last, the P/YPO_4 composite is obtained with an excess amount of red phosphorus.

Scheme 1 shows a formation mechanism for the hierarchical structure. The whole growth process follows an interfacial liquid–solid reaction between red P and YCl_3 aqueous solution. Initially, smooth spheres are formed from red phosphorus particles, which may be related to the synergetic effect of the shear stress from water and the reaction between YCl_3 and P. And then, needle-like YPO_4 is observed on the outer layer of the microspheres. As more YCl_3 solution diffuses into the sphere, the YPO_4 needles gradually evolve to sheets. Meanwhile, the hollow structure is formed with the consumption of red phosphorus. The growth process continues until YCl_3 is depleted, resulting in hierarchical hollow spheres composed of YPO_4 nanosheets and unreacted amorphous red phosphorus. The different microsphere sizes at different reaction times can be understood by the competition between the diffusion of YCl_3 and the consumption of red P. At the initial

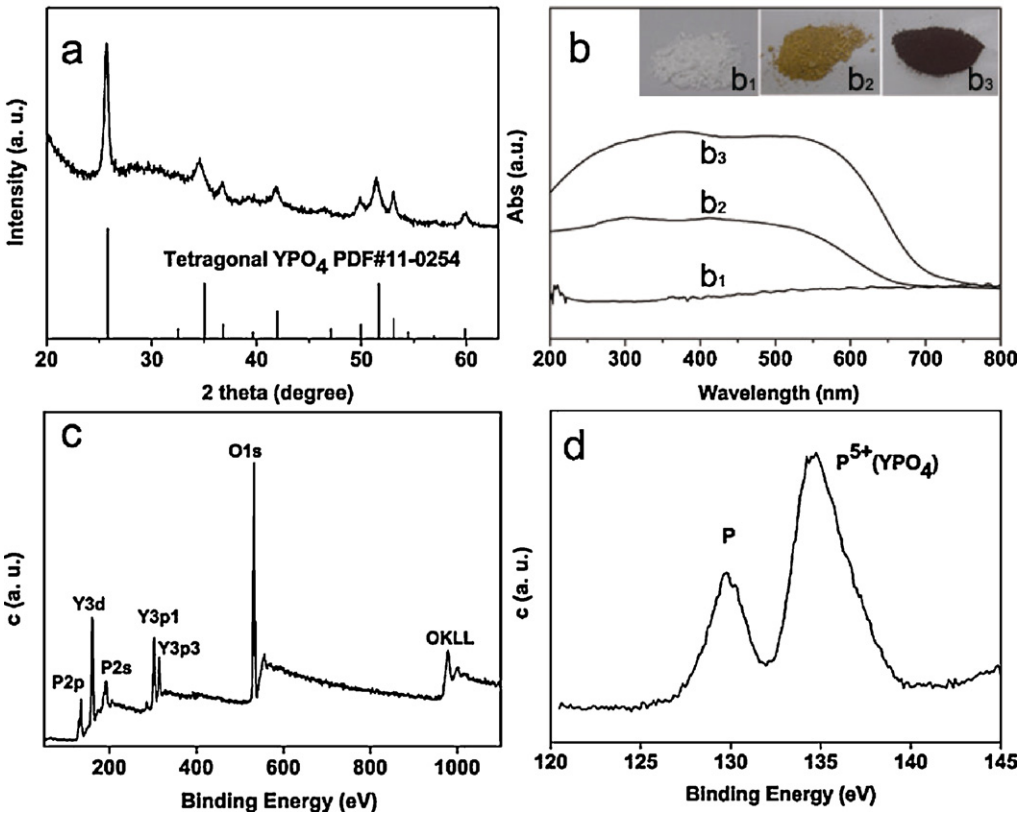

Fig. 1. (a) A typical XRD pattern of the P/YPO_4 composite, (b) UV–vis diffuse reflectance spectra of YPO_4 (b_1), P/YPO_4 (b_2) and red phosphorus (b_3), (c) a wide-range XPS spectrum and (d) a high-resolution P 2p XPS spectrum of P/YPO_4.

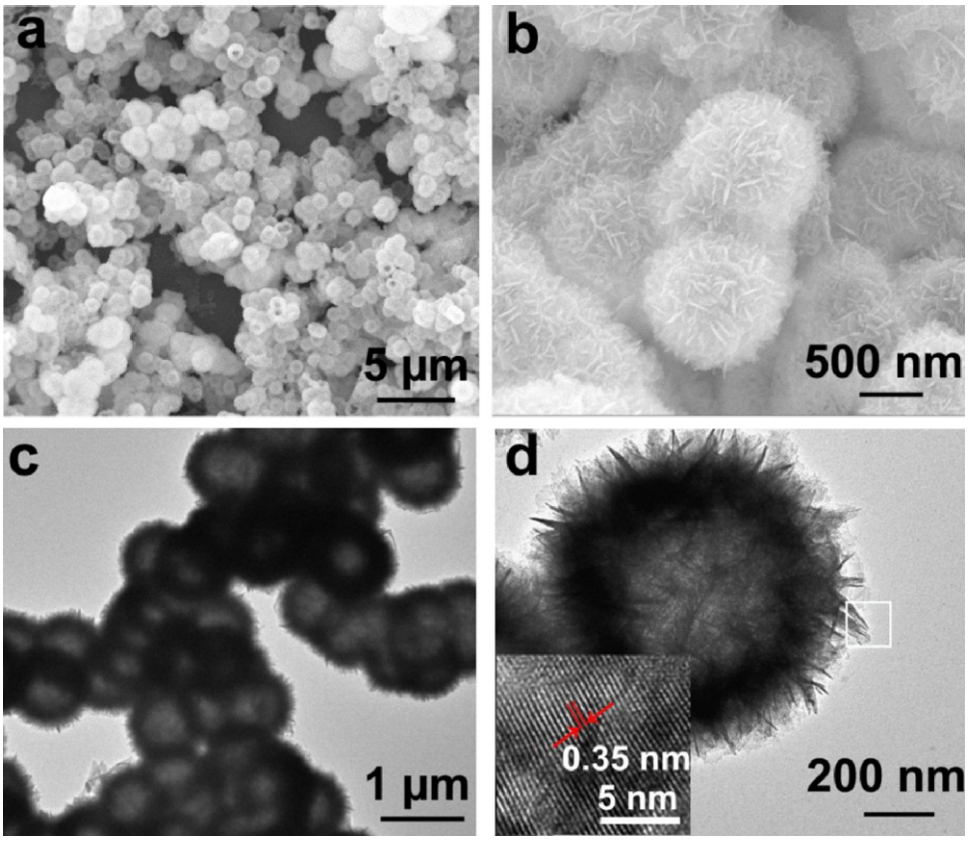

Fig. 2. (a, b) SEM and (c, d) TEM images of resulted hierarchical YPO_4/P hollow microspheres with different magnifications. Inset is the HRTEM image of the marked frame region in (d).

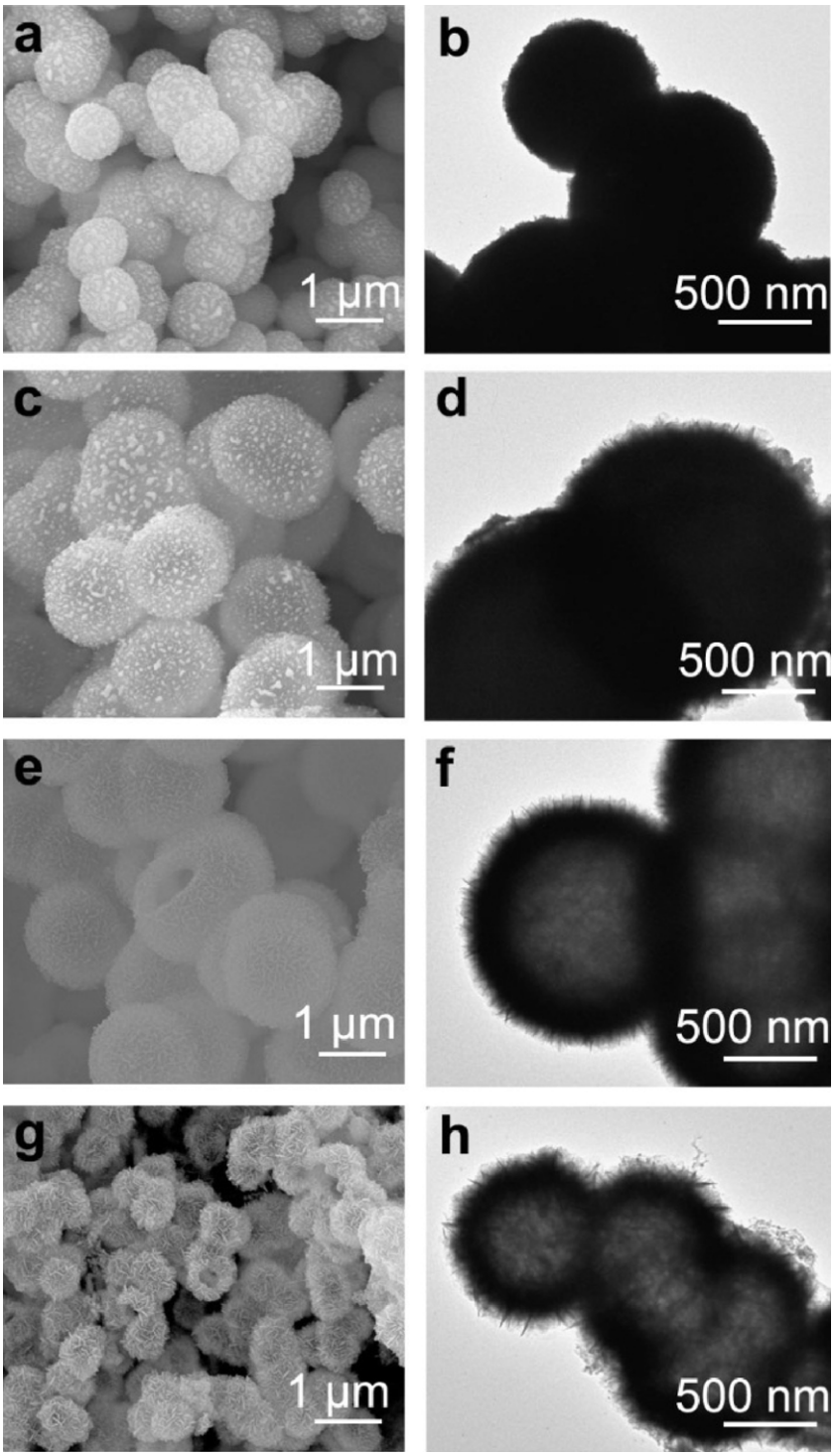

Fig. 3. (a, c, e, g) SEM and (b, d, f, h) TEM images of YPO_4/P composite at 0.5 h (a and b), 1.0 h (c and d), 5.0 h (e and f), 20.0 h (g and h).

stage of the reaction, the penetration of YCl_3 is dominated with the swelling of microsphere and the increase of the microsphere size. The following growth-ripen process with the consumption of red P decreases the size of microspheres.

A series of samples with different molar ratios of P to YPO_4 were fabricated for photocatalytic H_2 formation measurements and labeled as S1, S2, S3, S4 and S5, respectively (see Table 1). The actual chemical compositions of the samples were determined by TGC analysis. Fig. 4 shows the rate of H_2 formation on P/YPO_4 catalysts with different contents of YPO_4. Results indicate that YPO_4 has a great influence on the photocatalytic activity, though these samples possess similar BET surface areas and morphologies (Fig. S3). The rate of H_2 production increases with increasing the amount of YPO_4, and reaches a maximum value with 55 wt% YPO_4 (sample S2). The rate of H_2 formation for the composite with 55 wt% YPO_4 is ~6 times higher than that for red P.

To explain the enhanced photocatalytic activity and to elucidate the mechanism for the charge transfer in the P/YPO_4 photocatalyst, the band positions of YPO_4 were evaluated by measuring its water splitting activities under full spectrum irradiation from

Table 1
Synthesis conditions and physical properties of P/YPO_4 samples.

Samples		Red P	P/YPO_4 composites				
			S1	S2	S3	S4	S5
Synthesis condition	YCl_3 (mg)	0	300	300	300	300	300
	P (mg)	300	600	500	400	300	200
Percentages of YPO_4 (wt%)		0	40	55	67	78	92
UV absorption edge (nm)		700	700	700	700	700	700
BET surface area (m^2/g)		25.3	100.2	105.0	116.2	113.5	127.4
Pore distribution (nm)		1–100	1–100	2–100	7–100	10–100	10–100
Average pore size (nm)		8.7	17.8	19.7	26.0	30.3	34.5

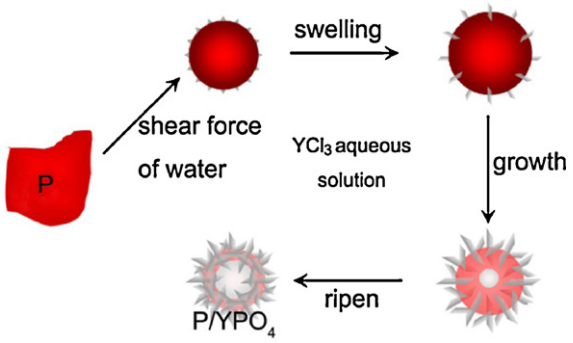

Scheme 1. The possible reaction and formation process of hierarchical P/YPO_4 hollow spheres.

a xenon lamp. Results indicated that YPO_4 was active for photocatalytic hydrogen production, but not active for oxygen formation. These findings imply that the conduction and valence bands of YPO_4 are more negative than the reduction and oxidation levels for H_2O. Knowing the band structures of red phosphorus [8], we propose that the photogenerated holes from red phosphorus are transferred to the valence band of YPO_4 in a P/YPO_4 composite, and thus separating the photogenerated carriers (Fig. S5). Together with an effective utilization of light by the hierarchical architecture [25], the composites exhibit a higher efficiency for photocatalytic H_2 production than that of red P.

For comparison, a sample was prepared by simply mixing P and YPO_4 to form a product with 55 wt% YPO_4. However, the mixture exhibits a photocatalytic H_2 production rate that is even lower than that of red phosphorus (Fig S4). This fact implies that in situ synthesis of P/YPO_4 composites is vital for the effective separation of the photogenerated carriers between P and YPO_4.

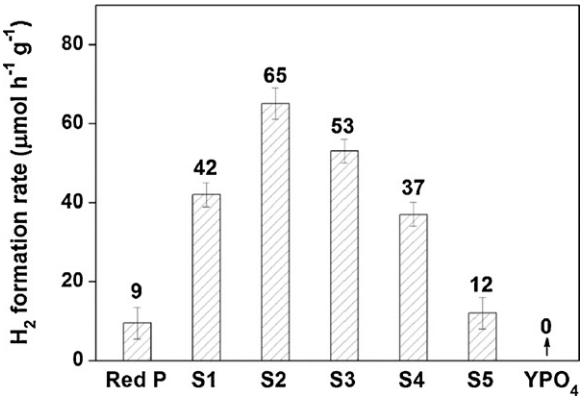

Fig. 4. Comparison of the photocatalytic H_2 formation of red P, P/YPO_4 and YPO_4 samples with 1 wt% Pt loaded under visible light irradiation (a 300 W xenon lamp with a 400 nm filter) using methanol aqueous solution.

4. Conclusion

In summary, hierarchical P/YPO_4 hollow microspheres were fabricated by the reaction between amorphous red phosphorus and YCl_3 aqueous solution via a hydrothermal method. The hierarchical architecture is composed of crystalline YPO_4 coupled with amorphous red P. The composite containing 53 wt% YPO_4 is up to 6 times more active than red phosphorus for photocatalytic hydrogen formation. The high photocatalytic activity is related to the effective separation of photogenerated carriers and the hierarchical structure.

Acknowledgments

Yeming Xu and Prof. Quan Li of the Department of Physics are gratefully acknowledged for their help in TEM characterization and valuable discussions. The work described in this paper was partially supported by the Focused Investments Scheme of The Chinese University of Hong Kong and a grant from the Research Grants Council of the Hong Kong Special Administration Region, China (Project 404810).

Appendix A. Supplementary data

Supplementary data associated with this article can be found, in the online version, at doi:10.1016/j.apcatb.2012.03.011.

References

[1] A. Fujishima, K. Honda, Nature 238 (1972) 37–38.
[2] K. Maeda, K. Teramura, D.L. Lu, T. Takata, N. Saito, Y. Inoue, K. Domen, Nature 440 (2006) 295.
[3] X.L. Hu, G.S. Li, J.C. Yu, Langmuir 26 (2010) 3031–3039.
[4] K. Maeda, K. Domen, J. Phys. Chem. C 111 (2007) 7851–7861.
[5] X.B. Chen, S.H. Shen, L.J. Guo, S.S. Mao, Chem. Rev. 110 (2010) 6503–6570.
[6] Z.G. Zou, J.H. Ye, K. Sayama, H. Arakawa, Nature 414 (2001) 625–627.
[7] F. Wang, W.K.H. Ng, J.C. Yu, H.J. Zhu, C.H. Li, L. Zhang, Z.F. Liu, Q. Li, Appl. Catal. B 111–112 (2012) 409–414.
[8] F. Wang, X. Chen, X. Hu, K.S. Wong, J.C. Yu, Sep. Purif. Technol. (2011), doi:10.1016/j.seppur.2011.10.027.
[9] B.T. Jonker, Y.D. Park, B.R. Bennett, H.D. Cheong, G. Kioseoglou, A. Petrou, Phys. Rev. B 62 (2000) 8180–8183.
[10] Y. Wu, J. Xiang, C. Yang, W. Lu, C.M. Lieber, Nature 430 (2004) 61–65.
[11] J. Zhang, Q. Xu, Z. Feng, M. Li, C. Li, Angew. Chem. Int. Ed. 47 (2008) 1766–1769.
[12] G.S. Li, D.Q. Zhang, J.C. Yu, Environ. Sci. Technol. 43 (2009) 7079–7085.
[13] J.R. Ran, J.G. Yu, M. Jaroniec, Green Chem. 13 (2011) 2708–2713.
[14] G. Liu, L.Z. Wang, H.G. Yang, H.M. Cheng, G.Q. Lu, J. Mater. Chem. 20 (2010) 831–843.
[15] X.G. Peng, Acc. Chem. Res. 43 (2010) 1387–1395.
[16] R. Buonsanti, V. Grillo, E. Carlino, C. Giannini, F. Gozzo, M. Garcia-Hernandez, M.A. Garcia, R. Cingolani, P.D. Cozzoli, J. Am. Chem. Soc. 132 (2010) 2437–2464.
[17] B.M. Barry, E.G. Gillan, Chem. Mater. 20 (2008) 2618–2620.
[18] J.L. Wang, Q. Yang, Z.D. Zhang, S.H. Sun, Chem. Eur. J 16 (2010) 7916–7924.
[19] B. Kraeutler, A.J. Bard, J. Am. Chem. Soc. 100 (1978) 4317–4318.

[20] X.C. Wang, K. Maeda, A. Thomas, K. Takanabe, G. Xin, J.M. Carlsson, K. Domen, M. Antonietti, Nat. Mater. 8 (2009) 76–80.
[21] K. Asami, H.M. Kimura, K. Hashimoto, T. Masumoto, A. Yokoyama, H. Komiyama, H. Inoue, J. Non-Cryst. Solids 64 (1984) 149–161.
[22] R. Franke, T. Chasse, P. Streubel, A. Meisel, J. Electron Spectrosc. 56 (1991) 381–388.
[23] D.M. Yost, H. Russell, Systematic Inorganic Chemistry of the Fifth-and-Sixth-Group Nonmetallic Elements, Prentice-Hall, Inc., New York, 1944, pp. 158–168.
[24] S. Hörold, 27th International Pyrotechnics Seminar, July 16–21, 2000.
[25] G.S. Li, D.Q. Zhang, J.C. Yu, Chem. Mater. 20 (2008) 3983–3992.